Lazy Quantum Walks with Native Multiqubit Gates

Steph Foulds¹ and Viv Kendon¹

¹Department of Physics, University of Strathclyde, Glasgow G4 0NG, UK*

Quantum walks, the quantum analogue to the classical random walk, have been shown to model fluid dynamics. Neutral atom hardware is a promising choice of platform for implementing quantum walks due to its ability to implement native multiqubit (\geqslant 3-qubit) gates and to dynamically rearrange qubits. Using error modelling for multiqubit Rydberg gates via two-photon adiabatic rapid passage, we present the gate sequences and predicted final state fidelities for some toy quantum walks, including 'lazy' quantum walks. These 'lazy' quantum walks include a rest state and therefore provide an integral step towards quantum walks for fluid simulation.

I. Introduction

Engineering, astrophysics, thermodynamics are among the many fields that utilise fluid mechanics simulations. Useful problems are usually impossible to solve analytically, and so classical solvers are used to simulate partial differentiation equations via discrete updates. This requires the relevant nonlinear algebraic equations to be constructed and solved on computers.

Discrete-time quantum walks (QWs) are the quantum analogue to the classical random walk: the movement of a walker on a d-dimensional lattice is dictated by the flip of a quantum 'coin' at each step [1, 2]. Due to the inference effects, quantum walks can exhibit exponentially faster hitting times [3, 4] and algorithmic speed-up [5, 6], indicating a possible advantage offered by QW-based search algorithms. The Dirac equation is known to be able to be obtained from the continuous limit of a d-dimensional QW [7–9]. More recently, 'lazy' open QWs have been shown to map to computational methods for fluid simulation such as lattice Boltzmann method [10], quantum fluid dynamics [11], and smoothed-particle hydrodynamics [12]. This work concerns evaluating the ability of near-term hardware to perform small, proof-of-concept quantum walks – but crucially with the inclusion of a rest state to encompass 'lazy' quantum walks [13], providing an integral step towards quantum walks for fluid simulation. One-dimensional quantum walks without a rest state have been implemented on a superconducting IBM device [14], a trapped-ion quantum processor [15], and a nuclear magnetic resonance (NMR) quantum processor [16].

Neutral atom hardware is a promising choice of platform for implementing quantum walks due to its ability to implement native multiqubit (\geq 3-qubit) gates and to dynamically re-arrange qubits [17]. In this work we employ quantum half-adder gate sequences to perform quantum walks, which require gates that act on at least three qubits, increasing with system size. Therefore native multiqubit gates drastically reduce the implementation's gate depth. Further, recent work [17] has shown that, largely due to the dynamically reconfigurable qubit connectivity, the predicted quantum volume metrics of neutral atom quantum processors are highly competitive against current superconducting circuit systems.

The aim of this paper therefore is to (1) highlight the utility of the native multiqubit gates and mid-circuit array programmability in the neutral atom platform and (2) guide the progress of neutral atom hardware with potential applications. Using error modelling for multiqubit Rydberg gates via two-photon adiabatic rapid passage [18], SPAM, and passive error [19], we present the gate sequences and final state fidelities for quantum walks with and without a rest state on 4 to 16-node rings.

II. Background

It has been shown [13] that discrete-time quantum walks (DTQWs) taken over the continuum limit – taking the time step and lattice spacing to zero with constant total time – can give efficient (linear in the total evolution time) simulations even when the Hamiltonian is not sparse. A smooth continuity between the discrete and continuous-time pictures requires the non-zero probability of a rest state, such that the walker can remain at the same lattice site for a time step [20, 21]. A QW with a rest state is denoted a 'lazy' QW.

Lazy open QWs can perform effective partial differential equations (PDEs) such as those governing Dirac-type dynamics to dispersive behaviour [22, 23]. Further, lazy QWs have been shown to map to computational methods

^{*} s.foulds@strath.ac.uk

for fluid simulation such as lattice Boltzmann method [10], quantum fluid dynamics [11], and smoothed-particle hydrodynamics [12].

Taking the smoothed-particle hydrodynamics (SPH) as an example, it has been shown [12] that one step of a lazy quantum walk $U = SC(\alpha)$ on the state $|\psi\rangle = \sum u_j |j\rangle \otimes |0\rangle$ is equivalent to the advection equation:

$$u_j(t+1) = u_j(t) \left(1 + \sum_k \alpha_{jk} \right) - \sum_k u_k(t) \alpha_{jk}$$
(1)

where the α can be tuned to SPH parameters via the coin operator $C(\alpha)$. Since the shift operator S depends only on the dimensionality of $|\psi\rangle$ and not the specific dynamics governed by α , we can investigate the shift operator S with arbitrary coin operator C for this application.

Therefore in this work we wish to evaluate the theoretical performance of the shift operator S on a neutral atom computer, as one component of an end-to-end PDE solver with quantum walks.

III. Methodology

In this work we exclusively use pure 2-dimensional qubits as inputs due to our model using near-term neutral atom qubits (see Section III C). A pure n-qubit composite state is represented by state vector [24]

$$|\psi\rangle = \sum_{\sigma \in \{0,1\}^{\otimes n}} A_{\sigma} |\sigma\rangle \tag{2}$$

where the probability of measuring bit string σ in the computational basis is $P(\sigma) = |\langle \sigma | \psi \rangle|^2$ where $\langle \sigma | \sigma' \rangle = \delta_{SS'}$. Output states may be mixed qubit states represented by $\rho_A = \operatorname{tr}_B(|\psi\rangle\langle\psi|_{AB}) = \sum_{j \in \{0,1\}^{\operatorname{len}(B)}} \langle j|_B |\psi\rangle\langle\psi|_{AB} |\psi\rangle_B$.

We define state fidelity in terms of the Hellinger distance [25, 26] between two probability distributions p and q:

$$H^{2} = \frac{1}{2} \sum_{z} \left(\sqrt{p(z)} - \sqrt{q(z)} \right)^{2}$$

$$= \frac{1}{2} \left(\sum_{z} p(z) + \sum_{z} q(z) \right) - \langle \sqrt{p} | \sqrt{q} \rangle$$
(3)

therefore we define our state fidelity [26] as

$$f = (1 - H^2)^2 (4)$$

$$= \left(1 - \frac{1}{2} \sum_{z} \left(\sqrt{P_{\text{ideal}}(z)} - \sqrt{P_{\text{eff}}(z)}\right)^{2}\right)^{2} \tag{5}$$

where $P_{\text{eff}}(z)$ is the probability of measuring z in a model with errors, and $P_{\text{ideal}}(z)$ is the probability of measuring z for an errorless model. The state fidelity is bounded by $0 \le f \le 1$ where f=1 denotes complete agreement between the two probability sets and f=0 denotes approximately orthogonal probability distributions – i.e. $\langle \sqrt{P_{\text{ideal}}} | \sqrt{P_{\text{eff}}} \rangle = \frac{1}{2} (\sum_{z} P_{\text{ideal}}(z) + \sum_{z} P_{\text{eff}}(z)) - 1$. We have chosen this measure in order to make a comparison with the results obtained in Ref [14].

We define gate fidelity with the limited tomography prescription [18]:

$$\mathcal{F}(U_{\text{eff}}) = |\langle \psi | U_{\text{eff}}^{\dagger} U_{\text{ideal}} | \psi \rangle|^{2}$$
(6)

where $|\psi\rangle = \frac{1}{\sqrt{2^m}} \sum_{s \in \{0,1\}^{\otimes m}} |s\rangle$. Gate fidelity is bounded by $0 \leqslant \mathcal{F} \leqslant 1$: if $\mathcal{F}(U_{\text{eff}}) = 1$ then $U_{\text{eff}} \equiv U_{\text{ideal}}$; if $\mathcal{F}(U_{\text{eff}}) = 0$ then the states $|\Psi\rangle = U_{\text{ideal}} |\psi\rangle$ and $|\Phi\rangle = U_{\text{eff}} |\psi\rangle$ are orthogonal.

A. One-qubit coin quantum walks

In this work we consider one dimensional quantum walks [27]. The 'walker' traverses an N-node line with position labels x s.t. $x \in \mathcal{Z}$ and $0 \le x < N$. In a physical system of qubits it is beneficial to encode the position state $|x\rangle$. In

this work we binary encode the position state with n qubits s.t. $x = 0 \to |x\rangle = |0\rangle^{\otimes n}$... $x = N - 1 \to |x\rangle = |1\rangle^{\otimes n}$. Therefore no physical walk is taking place, only an encoded one. For algorithmic convenience we also use cyclic boundary conditions such that x = (N - 1) + 1 = 0, so that the line becomes a ring.

Each step t of the walk, the coin is 'tossed' with coin operator C, and then the shift operator S moves the walker clockwise or anticlockwise on the line according to the coin state. The current state of the coin $|c(t)\rangle = A_0(t)|0\rangle + A_1(t)|1\rangle$ along with the current position state form the walker state $|\psi(t)\rangle = \sum_{x,c} A_{x,c}(t)|x,c\rangle$ with Hilbert space $\mathcal{H}_{xc} = \mathcal{H}_x \otimes \mathcal{H}_c$. The walker state evolves each step with $|\psi(t+1)\rangle = \mathrm{SC}_t |\psi(t)\rangle$, where [27]

$$S|x,0\rangle = |x-1,0\rangle \tag{7}$$

$$S|x,1\rangle = |x+1,1\rangle. \tag{8}$$

Encoded position rings and shift directions in state space and the physical qubits required to encode them are shown in Figure 1 (omitting anything in dashed purple) for four nodes and eight nodes.

Since we are interested primarily in the gate sequence to implementation of the shift operator, we define a simple, step independent coin operator which only acts on $|c\rangle$, of

$$C(t) = \mathbb{I}_N \otimes R_y(\theta_t) \equiv \mathbb{I}_N \otimes \begin{pmatrix} \cos\left(\frac{\theta_t}{2}\right) & -\sin\left(\frac{\theta_t}{2}\right) \\ \sin\left(\frac{\theta_t}{2}\right) & \cos\left(\frac{\theta_t}{2}\right), \end{pmatrix}$$
(9)

$$= \mathbf{C} = \mathbb{I}_N \otimes \mathbf{R}_y \left(\frac{\pi}{2}\right) \equiv \mathbb{I}_N \otimes \frac{1}{\sqrt{2}} \begin{pmatrix} 1 & -1\\ 1 & 1, \end{pmatrix}$$
 (10)

therefore:

$$C|x,0\rangle = \frac{1}{\sqrt{2}} (|x,0\rangle - |x,1\rangle), \qquad (11)$$

$$C|x,1\rangle = \frac{1}{\sqrt{2}}(|x,0\rangle + |x,1\rangle). \tag{12}$$

The value of θ_t dictates the probability of the walker maintaining the same shift direction, $P(c(t)|c(t-1)=c(t))=\cos^2\left(\frac{\theta_t}{2}\right)=\frac{1}{2}$, and of the walker changing direction, $P(c(t)|c(t-1)\neq c(t))=\sin^2\left(\frac{\theta_t}{2}\right)=\frac{1}{2}$, where we have chosen $\theta_t=\frac{\pi}{2}$ for simplicity.

The general circuit to perform a 2^n -node quantum walk [28] is shown in Figure 2. The shift operator has been split into 'increment' and 'decrement': the increment gates move the walker clockwise $(x \to x+1)$ if applied to state $|x,1\rangle$ and the decrement gates anticlockwise $(x \to x-1)$ if applied to $|x,0\rangle$. The shift operator acts on (n+1) qubits, composed of two each of the set of multiqubit gates $\{CkX|k \in \mathbb{N} \text{ and } 1 \ge k \ge n\}$, and $2n \times \mathbb{N}$ gates. Therefore, a (one-qubit coin) QW on a 2^n -node ring requires gates of rank $1 \ge r \ge n+1$, where the rank r of a gate is the number of qubits it acts on.

B. 'Lazy' two-qubit coin quantum walks

In order to increase the dimensionality of the coin to enact 'lazy' quantum walks, we encode the coin state $|c\rangle$ into 2 qubits with $c \in \{0,1\}^{\otimes 2}$ and the coin operator becomes $C^L(t) = \mathbb{I}_n \otimes R_y(\theta_t) \otimes R_y(\phi_t) = C^L = \mathbb{I}_n \otimes R_y(\frac{\pi}{2}) \otimes R_y(\frac{\pi}{2})$. The second coin qubit $|c_2\rangle$ and ϕ_t control the probability of the walker resting or moving $P(x(t) = x(t-1)) = P(c_2(t) = 0) = \cos^2(\frac{\theta_t}{2} = \frac{1}{2}, P(x(t) \neq x(t-1)) = P(c_2(t) = 1) = \frac{1}{2}$. The first coin qubit and θ_t controls the probability of changing or maintaining the shift direction with the same dynamics as the single-qubit (1q) coin walk, giving $P(c_1(t) = c_1(t-1)) = \frac{1}{4}$. Encoded position rings and shift directions, including the rest state, and the physical qubits required to encode them are shown in Figure 1 for a 4-node ring and an 8-node ring.

For a two-qubit coin the shift dynamics become

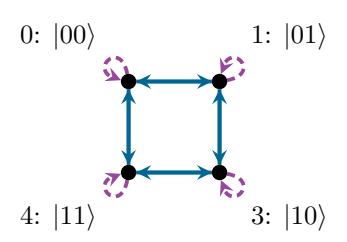
$$S|x,00\rangle = |x,00\rangle \tag{13}$$

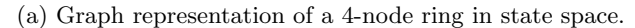
$$S|x,01\rangle = |x-1,01\rangle \tag{14}$$

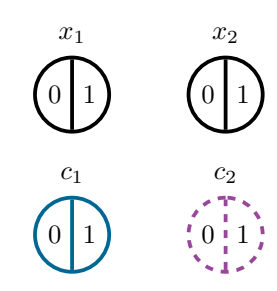
$$S|x,10\rangle = |x,10\rangle \tag{15}$$

$$S|x,11\rangle = |x+1,11\rangle. \tag{16}$$

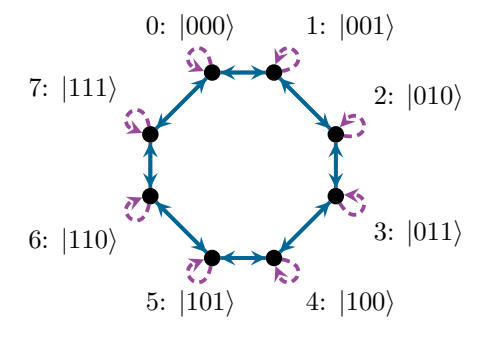
and therefore the shift operator for a two-qubit coin (2q-coin) quantum walk must be applied to (n+2) qubits. Figure



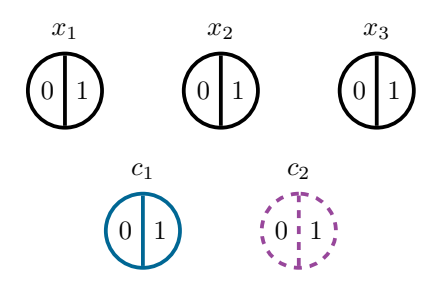




(b) Physical qubits for a 4-node ring.



(c) Graph representation of a 8-node ring in state space.



(d) Physical qubits for an 8-node ring.

Figure 1: Binary position and coin encodings for a 2^n -node ring, with the 2^n position nodes on the left encoded by the n physical qubits x_j in black on the right. Arrows denote available shift directions around the ring for a 2-qubit coin/'lazy' QW: the solid blue clockwise and anticlockwise directions are encoded by the solid blue physical qubit c_1 , and the dashed purple rest state is encoded by the dashed purple physical qubit c_2 . Omission of c_2 and therefore the rest state yields a 1-qubit coin/'non-lazy' QW.

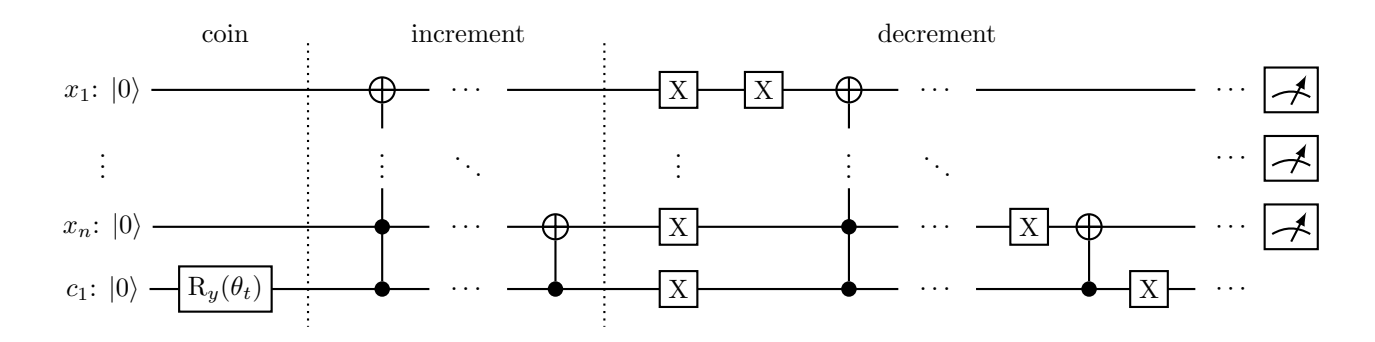


Figure 2: Gate circuit for one-qubit coin (1q-coin) quantum walk on a 2^n -node ring [28].

3 shows the general circuit for 2^n -node 2q-coin quantum walks – the gates from the respective 1q-coin circuits are controlled on both coin qubits, with the exception of the one-qubit X gates as the controls cancel out. Therefore, a 2q-coin QW on a 2^n -node ring requires gates of rank one and of rank $3 \le r \le n+2$. In general, an n_c -qubit coin QW on a 2^n -node ring requires gates of rank one and of rank $1 + n_c \le r \le n_q$ where $n_q = n + n_c$.

C. Neutral atoms

The Strathclyde neutral atom hardware has a programmable 2D array of Cs atoms trapped in a triangular array separated by $d \approx 5 \mu m$ at T = 0 K [18]. The hyperfine state $|1\rangle$ is coupled to a Rydberg state $|r\rangle$ via a two-photon transition (through an intermediate excited state $|e\rangle$). Rydberg states experience dipole-induced pairwise interaction; within the blockade distance there can only be one Rydberg excitation. Native multiqubit gates are $C_k Z$ gates with

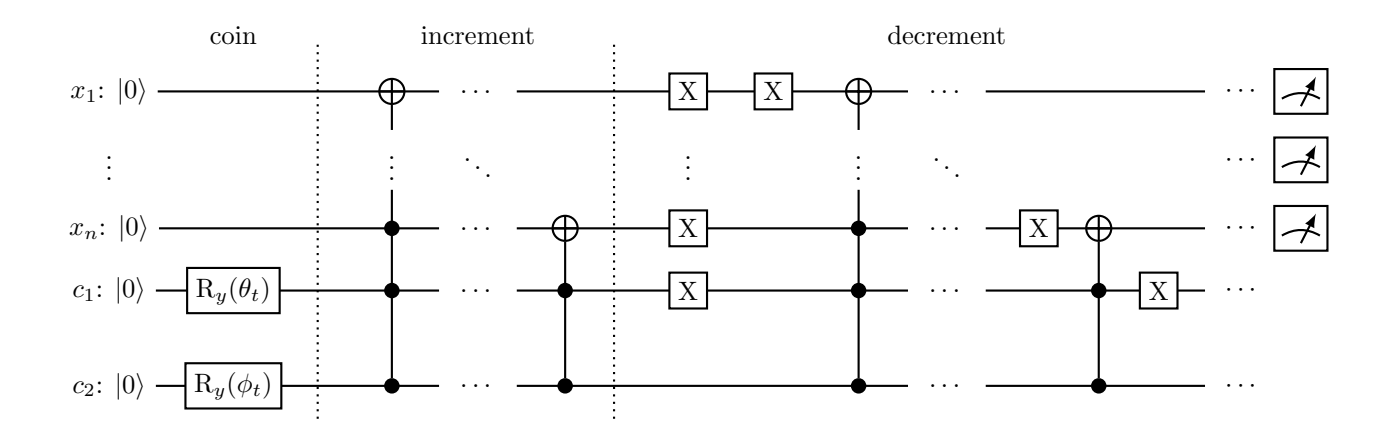


Figure 3: Gate circuit for a two-qubit coin (2q-coin) quantum walk on a 2^n -node ring.

ideal matrices

$$CkZ_{ideal} = |0\rangle^{\otimes(k+1)} \langle 0|^{\otimes(k+1)} - \sum_{\sigma \in \{0,1\}^{\otimes(k+1)}} |\sigma\rangle\langle\sigma|$$
(17)

acting on k+1 qubits. By convention this is denoted a $C_k Z$ gate however all k+1 qubits are controlled on and all k+1 qubits are acted on. This $C_k Z$ gate is achieved with two ARP (adiabatic rapid passage) [18, 29] pulses and a global single-qubit rotation $Z(\phi)$.

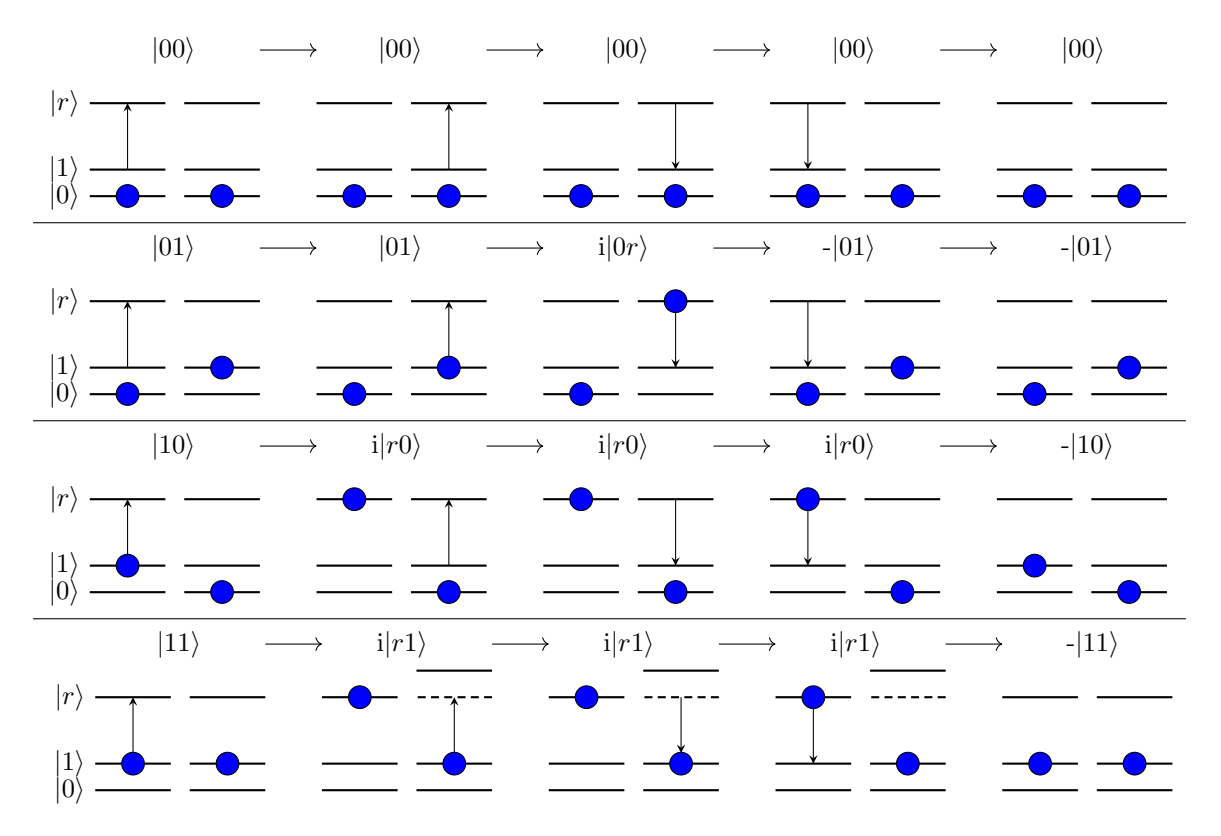


Figure 4: Pulse sequence for a CZ gate.

As shown in figure 4 with the example of the CZ gate, each atom is addressed in turn. If the atom currently addressed is in the $|1\rangle$ state, then it is excited up to the Rydberg state $|r\rangle$ – however if there is already an atom within the blockade radius in state $|r\rangle$ then the state is detuned and the addressed atom's energy level drops back down to

 $|1\rangle$. The state of any atom that reaches the Rydberg level is phased flipped. After all atoms have been address, the atoms are then again addressed in turn to drive the states in $|r\rangle$ back down to $|1\rangle$.

In this work we consider near-term gate modelling based on the work of Ref [18]. Considering an array of Cs atoms and current technologies, they use a detailed model that accounts for the effects of spontaneous decay and AC Stark shifts for experimentally feasible parameters. They therefore obtain realistic parameters for native two-qubit and multiqubit gates, with effective matrices [18]:

$$CZ_{\text{eff}} = |00\rangle\langle00| + 0.9990e^{0.9906i\pi} (|01\rangle\langle01| + |10\rangle\langle10|) + 0.9986e^{i\pi} |11\rangle\langle11|$$

$$CCZ_{\text{eff}} = |000\rangle\langle000| + 0.9981e^{0.9845i\pi} (|001\rangle\langle001| + |010\rangle\langle010| + |100\rangle\langle100|)$$

$$+ 0.9973e^{0.9934i\pi} (|011\rangle\langle011| + |101\rangle\langle101| + |110\rangle\langle110|) + 0.9963e^{0.9911i\pi} |111\rangle\langle111|.$$
(19)

Although further-term from CZ and CCZ gates, they also present the theoretical effective matrix for the C3Z gate [18]:

$$C3Z_{\text{eff}} = |0000\rangle\langle0000| + 0.997947e^{-0.995i\pi} \sum_{\sigma \in \mathbf{H}_{1}^{4}} |\sigma\rangle\langle\sigma| + 0.996286e^{0.984i\pi} \sum_{\sigma \in \mathbf{H}_{2}^{4}} |\sigma\rangle\langle\sigma| + 0.994391e^{0.981i\pi} \sum_{\sigma \in \mathbf{H}_{3}^{4}} |\sigma\rangle\langle\sigma| + 0.990724e^{0.981i\pi} |1111\rangle\langle1111|$$
(20)

where \mathbf{H}_a^4 is the set of all bit strings of length 4 with Hamming weight a (aka a number of 1s). Therefore the gate fidelity of each is $\mathcal{F}(\mathrm{CZ}_{\mathrm{eff}}) = 0.9981$, $\mathcal{F}(\mathrm{CCZ}_{\mathrm{eff}}) = 0.9954$, $\mathcal{F}(\mathrm{C3Z}_{\mathrm{eff}}) = 0.9850$. (In a native two-qubit gate setting these multigate fidelities could be recovered [30] with two-qubit gate fidelities of $\mathcal{F}(\mathrm{CZ}) = \sqrt[5]{\mathcal{F}(\mathrm{CCZ}_{\mathrm{eff}})} = 0.9991$ and $\mathcal{F}(\mathrm{CZ}) = \sqrt[20]{\mathcal{F}(\mathrm{C3Z}_{\mathrm{eff}})} = 0.9992$.)

A CkX gate can therefore be implemented with the addition of single qubit gates:

$$CkX = (R_z^{2\pi})^{\otimes k+1} (Z^{\otimes k} \otimes ZHZ) CkZ (R_z^{2\pi})^{\otimes k+1} (Z^{\otimes k} \otimes ZHZ)$$
(21)

where the target is the last qubit, where $R_z^{2\pi} \equiv -I_2$ and $H \equiv \frac{1}{\sqrt{2}} \begin{pmatrix} 1 & 1 \\ 1 & -1 \end{pmatrix}$. Since single-qubit gates have negligible error compared to multi-qubit gates ($\mathcal{F}(H,Z,X) = 0.9999$), we take one-qubit gates to have unity fidelity, and therefore $\mathcal{F}(CkX) = \mathcal{F}(CkZ)$.

Experimental implementation in a neutral atom setting have achieved gate fidelities of $\mathcal{F} = 0.9999$ for single qubit gates [31], $\mathcal{F} = 0.9950$ for two-qubit gates [29, 32], and $\mathcal{F} = 0.8704$ for three qubit gates [29]. Neutral atom arrays of >6000 trapped qubits have been demonstrated [33].

Further errors considered in this work are state preparation, readout, waiting times, and qubit movement.

At the start [17] of every QW each qubit is subject to error $\epsilon_{init} = 0.003$, and for a simulation of t steps, each qubit is subject to error $\epsilon_{read} = 0.0017$ at the end [19]. This error is modelled as population loss and is applied simply with the non-unitaries $E(\epsilon) = (1 - \epsilon)\mathbb{I}$.

During the walk, qubits may need to be moved to a different space in the array in order to interact with the required qubits. If this movement is performed slowly enough $-v \leq 0.55 \mu m/\mu s$ – then no fidelity penalty is incurred [19]. Therefore (below this speed) the only affect of movement is the passive noise experienced by the other qubits due to waiting time.

Passive noise, the effect of decay processes while a qubit is waiting to be acted on, is modelled as the longitudinal relaxation time decay with amplitude damping. The waiting error per qubit per step is therefore [34]:

$$\epsilon_{\text{wait}}(\Delta t) = 1 - \exp\left[-\frac{\Delta t}{T_1}\right]$$
(22)

for duration Δt where $T_1 = 4s$ is the relaxation time. For qubits waiting during a gate $\Delta t = \tau_{\text{gate}} = 1.8 \mu s$ [18]. For qubits waiting during a movement $\Delta t = \tau_{\text{move}} = 100 \mu s$, which allows for $55 \mu m$ of errorless movement, which is far above sufficient for all mapped out moves on a $\sim 5 \mu m$ trap array. (See appendix for movement scheme for each size QW.) During each gate G, error $\epsilon_{\text{wait}}(\tau_{\text{gate}})$ is applied to every qubit not being acted on by that gate such that $\mathbb{I}_{2^a} \otimes G \otimes \mathbb{I}_{2^b}$ becomes $E(\epsilon_{\text{wait}})^{\otimes a} \otimes G \otimes E(\epsilon_{\text{wait}})^{\otimes b}$. For simplicity, every qubit undergoes waiting error during a movement with $E(\epsilon_{\text{wait}}(\tau_{\text{move}}))$.

D. Gate decompositions

We consider circuits with $(r \le 6)$ -qubit gates, but are only considering the implementation of native gates of rank $r \le 3$ for near-term and $r \le 4$ for further term implementation on neutral atom hardware – therefore many considered circuits must be decomposed into equivalent gate sequences composed of gates of a lesser rank. Examples of gate decompositions [30] are shown in Figure 5. A decomposition of a CkX gate into CCX gates requires 4(k-2) CCX gates and k-2 ancilla qubits. Decomposing a C4X(C5X) gate into native gates of rank $r \le 4$ requires two(zero) CCX gates, two(four) C3X gates, and one ancilla qubit.

The decomposition of each circuit used in this work are shown in the appendix.

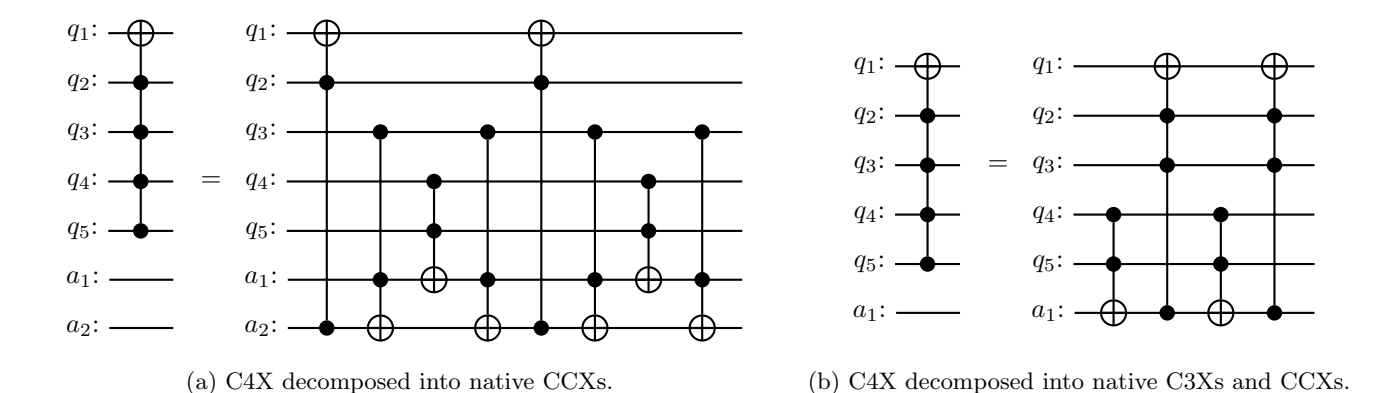


Figure 5: Gate decomposition examples [30] for C4X. Qubits q_j are qubits undergoing the gate operation and qubits a_j are ancilla.

IV. Results

A. Near-term

We perform a numerical simulation (on a laptop with an Intel core i5 processor) of 21 steps of one-qubit coin (1q-coin) and two-qubit coin (2q-coin) QWs on a 2^n -node ring for $2 \ge n \ge 4$, using the gate circuits in Appendix A. Gate errors, passive noise, state preparation, and readout are modelled as described in Section III C. For simplicity, the coin parameters are static with $\theta_t = \phi_t = \frac{\pi}{2}$ for all t. In this section, we consider 'near-term' implementations and therefore use the native gate set $\mathbf{G}(\max(r) = 3) = \{H, X, R_y(\frac{\pi}{2}), CZ_{\text{eff}}, CCZ_{\text{eff}}\}$.

Final state fidelity against number of steps are shown in Figure 6, along with the IBM implementation in Wadhia et al. [14] for comparison. Note that only the results for the 1q-coin QWs are available for the IBM comparison. It is clear that the overriding factor in state fidelity per step is the maximum rank of the gates in the QW gate circuit prior to decomposition, equivalent to the total number of position qubits and coin qubits: $n_q = n+1$ for 1q-coin QWs and $n_q = n+2$ for 2q-coin QWs. In general, the state fidelity decreases as n_q increases. Further, the fidelity curves for QWs with equal n_q values are roughly equivalent: 2q-coin QWs on a 2^n -node ring results match those for 1q-coin QWs on a 2^{n+1} -node ring.

The gate errors contribute overwhelmingly to state fidelity loss – with only gate errors considered, the increase in fidelity is only 0.017 - 0.17 % for the 1q-coin QW on a 4-node ring (roughly increasing as number of steps increases).

The walks with final state fidelities within tolerances $\{0.99, 0.999, 0.9999\}$ after t steps are: QWs with $n_q=3$ qubits (1q-coin QW on a 4-node ring) are within 0.99 for 7 steps and 0.999 for 2 steps; QWs with $n_q=4$ qubits (2q-coin QW on a 4-node ring and 1q-coin QW on an 8-node ring) are within 0.99 for 4 steps; and QWs with $n_q=5$ qubits (2q-coin QW on an 8-node ring and 1q-coin QW on a 16-node ring) are within 0.99 for 1 step. After one step the 2q-coin QW on a 16-node ring has state fidelity 0.981, and therefore is within none of these tolerances for any number of steps; after one step the 4-node with 1q-coin has state fidelity 0.9997 and therefore none of the QWs are within tolerance 0.9999 for any steps. (Note that the state fidelity as a function of the number of steps is subpolynomial for the first few steps, which is much more noticeable for the 2q-coin QW on a 16-node ring.)

Therefore of those considered, the only QWs feasible – which here we mean which have state fidelity within tolerance 0.99 for at least four steps – are (1q- or 2q-coin) QWs on a 4-node ring or 1q-coin QWs on a 8-node ring. 1q-coin

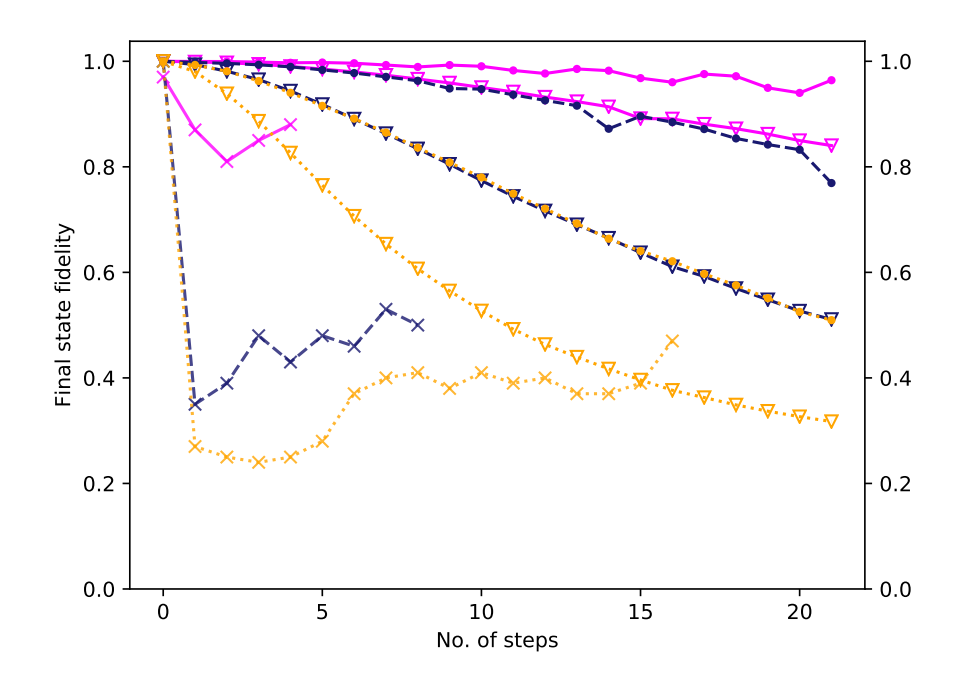


Figure 6: Final fidelity of the final position states between errorless and simulated error 1q-coin (circles) and 2q-coin (triangles) QWs on 2^n -node rings, using native gate set $\mathbf{G}(\max(r) = 3)$. Pink solid lines denote QWs on 4-node rings, dashed blue on 8-node rings, and dotted gold lines on 16-node rings. IBM results (using native gates of $\max(r) = 2$) [14] for 1q-coin QWs are also shown for comparison in crosses.

QWs on a 4-node ring have the added benefit of maintaining state fidelity above 0.9 for at least 21 steps.

B. Further term

We wish to identify the best potential hardware improvements for the application on 1q-coin and 2q-coin QWs. First we incorporate the use of the 4-qubit gate C3Z with the effective matrix from equation 20, expanding our native gate set to $\mathbf{G}(\max(r)=4)=\{\mathrm{H},\mathrm{X},\mathrm{R}_y(\frac{\pi}{2}),\mathrm{CZ}_{\mathrm{eff}},\mathrm{CCZ}_{\mathrm{eff}},\mathrm{C3Z}_{\mathrm{eff}}\}$. Figure 7 shows the final state fidelities for the considered QWs with this gate set, along with the previous section's results with gate set $\mathbf{G}(r\leqslant3)$ in reduced opacity for comparison. This increase in $\max r$ provides a percentage increase of $\sim28\%$ in the state fidelity for the 2q-coin QW on a 4-node ring after 21 steps. Due to the greater asymmetry in C3Z_{eff} as opposed to the other effective matrices (see Equations 18-20), the fidelity curves are much less smooth.

Although at large (> 10) numbers of steps the improvement in state fidelity is significant, for few steps there is only slight improvement. The number of steps within state fidelity tolerance 0.99 for QWs with native gate set $\mathbf{G}(r \leq 4)$ increase to 5 from 2 steps with $\mathbf{G}(r \leq 3)$, but otherwise there are no step increases for tolerances $\{0.99, 0.999, 0.9999, 0.9999\}$.

Another route is to improve the gate fidelities of CZ and CCZ. In order to model further term gate fidelities we construct effective matrices

$$CZ(a) = \operatorname{diag}\left[1, \ \alpha_1(a)e^{i\pi\phi_1(a)}, \ \alpha_1(a)e^{i\pi\phi_1(a)}, \ \frac{\alpha_2(a=0)}{\alpha_1(a=0)}\alpha_1(a)e^{i\pi\frac{\phi_2(a=0)}{\phi_1(a=0)}\phi_1(a)}\right]$$
(23)

where $\alpha_1(a) = 0.9990 + 0.0001a \le 1$, $\phi_1(a) = 0.9906 + 0.0010a \le 1$, and $CZ(a = 0) = CZ_{eff}$. Therefore the ratio between gate coefficients is maintained. We similarly construct CCZ(a), and only consider gate pairs [CZ(a), CCZ(a)]. Figure 8 shows the final state fidelities for 1q-coin and 2q-coin QWs on a 4-node ring with native gate sets

Figure 8 shows the final state fidelities for 1q-coin and 2q-coin QWs on a 4-node ring with native gate sets $\mathbf{G}(\max(r)=3)(a)=\{\mathrm{H},\mathrm{X},\mathrm{R}_y(\frac{\pi}{2}),\mathrm{CZ}(a),\mathrm{CCZ}(a)\}$ where $a\in\{0,\frac{13}{3},\frac{26}{3},13,\frac{52}{3},\frac{65}{3},26\}$. Note that the troughs in the state fidelity curves are due to phase values $\phi_j(a)\neq 1$, however they become less significant as the coefficients $\alpha_j(a)$ approach unity. The sudden jump in smoothness found with gate fidelities $[\mathcal{F}(\mathrm{CZ}),\mathcal{F}(\mathrm{CCZ})]=[99.99,99.79]\%$ which corresponds to $\alpha_1(a)=1$.

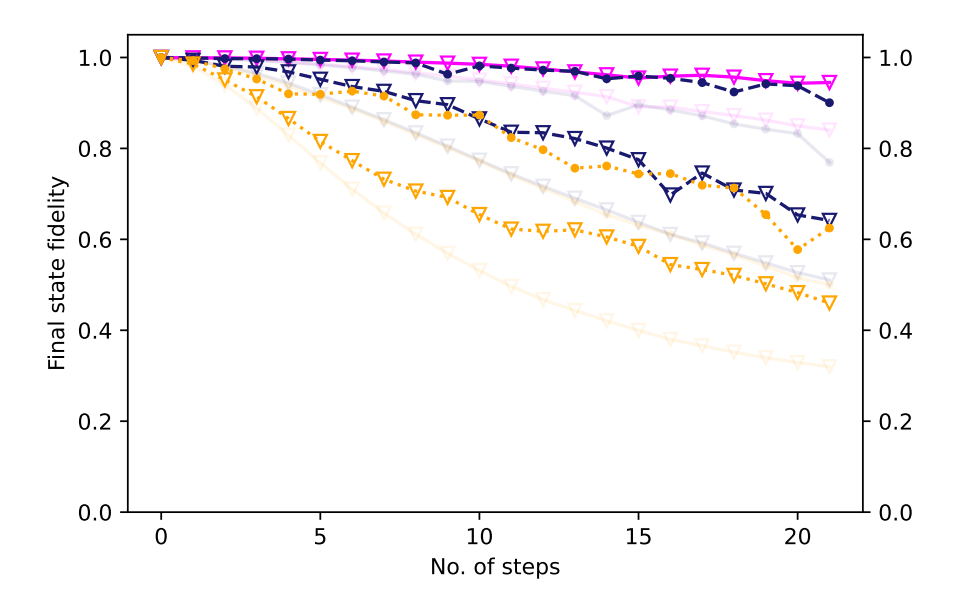


Figure 7: Final fidelity of the position states between errorless and simulated error QWs with native gate set $\mathbf{G}(\max(r)=4)$. Circles denote 1q-coin QWs, and triangles 2q-coin QWs. Pink solid lines are on 4-node ring, dashed blue on 8-node rings, and dotted gold lines on 16-node rings. In low opacity are the results of QWs with native gate set $\mathbf{G}(\max(r)=3)$ for comparison.

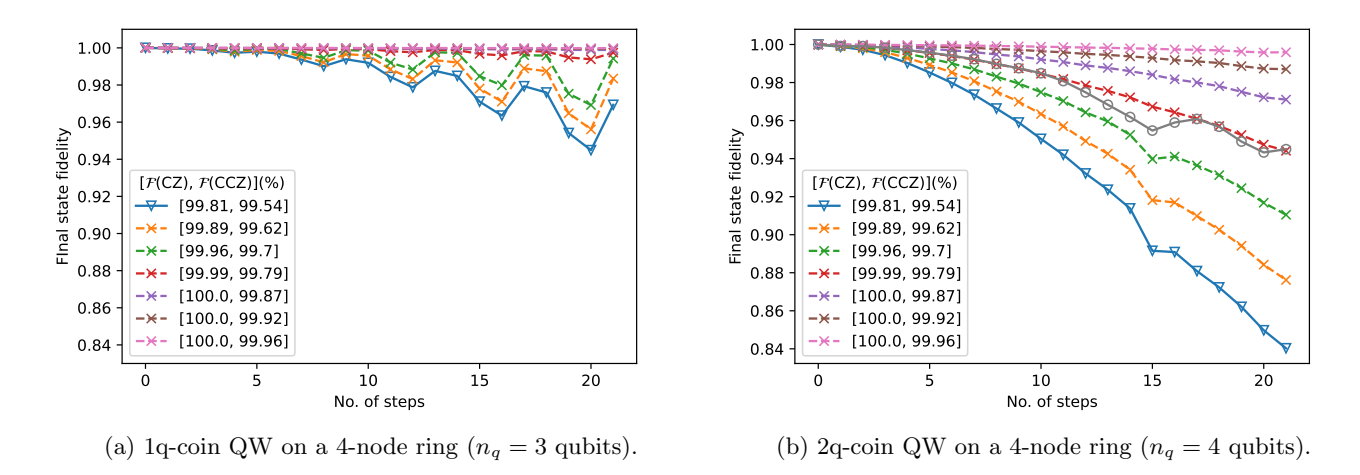


Figure 8: Final state fidelity at each step QWs on a 4-node ring using native gate set $\mathbf{G}(\max(r) = 3)(a)$ with various gate fidelities $\mathcal{F}(\text{CCZ})$ and $\mathcal{F}(\text{CZ})$. Also shown, for the 2q-coin QW, are the results using native gate set $\mathbf{G}(\max(r) = 4)$ in circles for comparison.

Further, Figure 9 shows the tolerance plots for these QWs. It can be seen that even for optimistic further-term gate fidelities $\mathcal{F}(CZ) = 99.96\%$ and $\mathcal{F}(CCZ) = 99.70\%$, only the 1q-coin QW on a 4-node ring has tolerance 0.999 after *one* step, and for the 2q-coin QW the error is under tolerance 0.99 for only 2 steps.

On Figure 8(b) we have also plotted the $\mathbf{G}(\max(r)=4)$ gate set result for comparison: we can see that it roughly aligns with the gate set $\mathbf{G}(\max(r)=3)(a=13)$ with $\mathcal{F}(\mathrm{CZ})=99.99\%$ and $\mathcal{F}(\mathrm{CCZ})=99.79\%$. These CZ and CCZ gate fidelities are also required for the number of steps within tolerance results to match. Similarly, for a 1q-coin QW on an 8-node ring, the state fidelity curve roughly matches that with $\mathcal{F}(\mathrm{CZ})=99.98\%$ and $\mathcal{F}(\mathrm{CCZ})=99.75\%$ – however to duplicate the number of steps within tolerance only gate fidelities $\mathcal{F}(\mathrm{CZ})=99.86\%$ and $\mathcal{F}(\mathrm{CCZ})=99.59\%$ are needed.

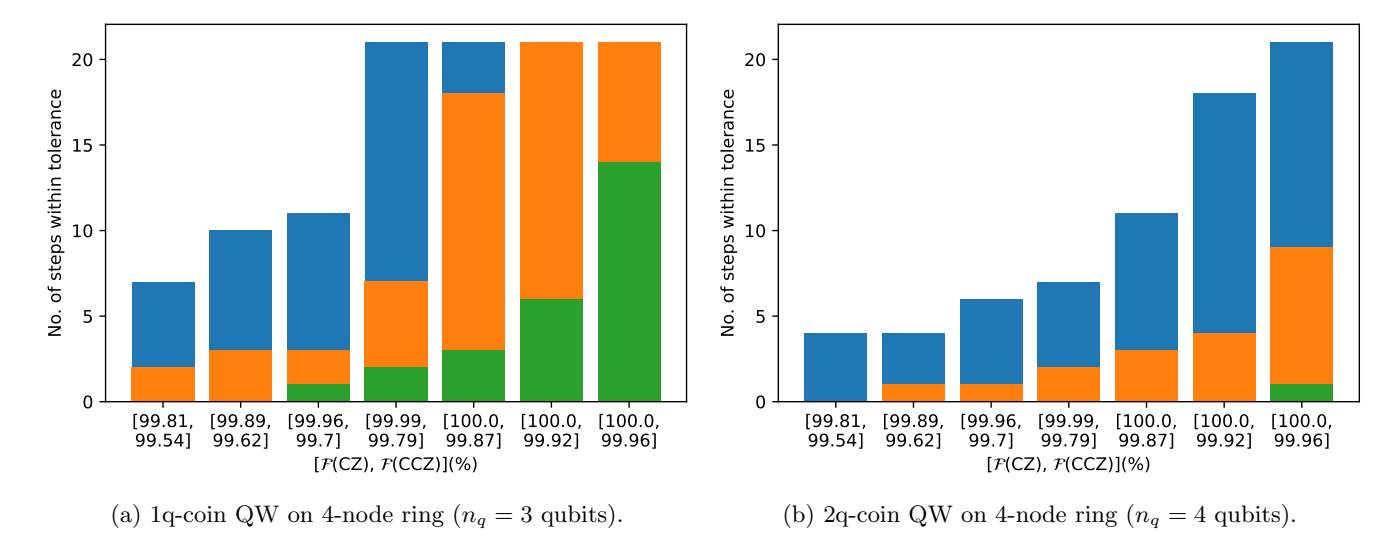


Figure 9: Number of steps for which the final state fidelity is within tolerance $\{0.99 \text{ (blue)}, 0.999 \text{ (orange hatched)}, 0.9999 \text{ (green dotted)}\}$ using native gate set $\mathbf{G}(\max(r) = 3)(a)$ with various gate fidelities $\mathcal{F}(\text{CCZ})$ and $\mathcal{F}(\text{CZ})$.

V. Conclusions

We show that with projected gate fidelities of $\mathcal{F}(\mathrm{CZ}) = 0.9981$ and $\mathcal{F}(\mathrm{CCZ}) = 0.9954$, a quantum walk with no rest-state performed on a 4-node ring (requiring three qubits) results in final state fidelity f > 0.99 after four time steps and f > 0.90 after twenty timesteps. More resource intensive quantum walks performed with these projected gate fidelities do not meet these tolerances. However, the additional use of a four-qubit C3Z gate with projected fidelity $\mathcal{F}(\mathrm{C3Z}) = 0.9850$ results in these tolerances met when performing a quantum walk with rest state on a 4-node ring or a quantum walk without rest state on an 8-node ring (both requiring four qubits). This, along with results of the model with improved two- and three-qubit gate fidelities, leads us to conclude that a native four-qubit gate and mid-circuit qubit array rearrangement is required for the implementation of interesting quantum walks on neutral atom hardware.

As we look to the further term and the goal of implementing larger (requiring more than five qubits) and more useful QWs, this raises the concern that QWs on 2^n -node ring require native gate ranks (number of qubits acted on) of at least n+1. We perform a back of the envelope calculation to find composite fidelities $f(\max(r)) = \prod_{k=2}^{\max(r)-1} \mathcal{F}(CkZ)^{\text{no. of }CkZ}$ for a two-qubit coin quantum walk on a 2^n -node ring for various n and various native gate sets $\mathbf{G}(\max(r)) = \{CkZ|2 \le k < \max(r)\}$, shown in Figure 10, where $\max(r)$ is the maximum rank of the gates in the gate set. Gate fidelities considered are $\mathcal{F}(CkZ) \in \{0.991, 0.992, 0.993]\}$ or $\{0.99, 0.995, 0.999\}$ or $\{0.99991, 0.99992, 0.99993\}$, such that $\mathcal{F}(C(k+1)Z) \le \mathcal{F}(CkZ)$ and the percentage increase is positive. There is a clear advantage in increasing the gate set from $\mathbf{G}(\max(r) = 3)$ to $\mathbf{G}(\max(r) = 4)$ – this advantage however is not as pronounced for further increases in gate sets. The average percentage increase of the composite fidelity with $\mathbf{G}(3 \to 4)$ is $\{23, 260, 4200, 270000\}$ % for $n \in \{5, 10, 15, 20\}$ respectively, as opposed to $\{4.0, 7.2, 12, 16\}$ % for $\mathbf{G}(4 \to 5)$. Therefore, while the introduction of C3Z gates would yield relatively large final state fidelity increases, it is not necessary to continue increasing native gate ranks ad infinum, and indeed $\max(r) = 4$ seems to be the sweet spot.

Further work can be split into theory and experiment. For the theoretical implementation, position encoding with Gray codes should be consider to potentially decrease the gate requirements. Only qubits were considered; the use of qutrit coins could also decrease gate requirements, although careful consideration of qutrit gate operation would be required. No error correction was considered; with the advent of fault-tolerant protocols for multiqubit gates [35], this should be added to the error model. With the specific view of the application to fluid simulation, we wish to extend the linear case considered in this work to the non-linear case by entangling the coin qubit(s) with an additional ancilla. Further term, we look to the extension of quantum walks on 1D rings to those on 2D lattices.

For experimentalists, we would like to see a quantum performed on a 4-node ring in order to compare our theoretical results. We would recommend the implementation of C3Z gates before any larger and therefore more application-relevant quantum walks are attempted.

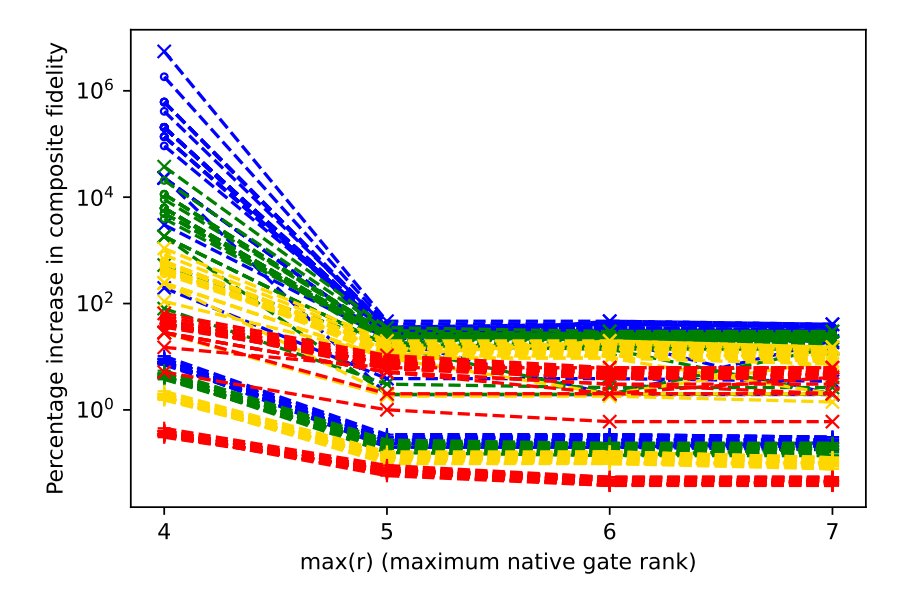


Figure 10: Percentage increase in composite fidelity $f(\max(r)) = \prod_{k=2}^{\max(r)-1} \mathcal{F}(Ck\mathbf{Z})^{\text{no. of }Ck\mathbf{Z}}$ from using native gate set $\mathbf{G}(\max(r))$ compared to using gate set $\mathbf{G}(\max(r)-1)$, with the number of multiqubit gates required for one step of a 2q-coin QW on a 2^n -node ring, where $n \in \{5, 10, 15, 20\}$ in red circles, gold pluses, green crosses, and blue dots respectively.

Acknowledgments

Thank you to Kathryn Lund, Gerard Pelegrí, and Lara Janiurek for interesting discussions and vital expertise. SF and VK funded by UKRI EPSRC grants EP/T026715/2, EP/T001062/1, EP/W00772X/2, and EP/Y004566/1, EP/Z53318X/1, and the UKRI DRI and STFC funded CCP-QC Bridge Project – extended case studies for neutral atom hardware.

- [1] Y. Aharonov, L. Davidovich, and N. Zagury, "Quantum random walks," Phys. Rev. A 48, 1687–1690 (1993).
- [2] Andris Ambainis, "Quantum walks and their algorithmic applications," (2004), arXiv:quant-ph/0403120 [quant-ph].
- [3] Andrew M. Childs, Edward Farhi, and Sam Gutmann, "An example of the difference between quantum and classical random walks," Quantum Information Processing 1, 35–43 (2002).
- [4] Julia Kempe, "Quantum random walks hit exponentially faster," (2002), arXiv:quant-ph/0205083 [quant-ph].
- [5] Andrew M. Childs, Richard Cleve, Enrico Deotto, Edward Farhi, Sam Gutmann, and Daniel A. Spielman, "Exponential algorithmic speedup by a quantum walk," in *Proceedings of the thirty-fifth annual ACM symposium on Theory of computing*, STOC03 (ACM, 2003) p. 59–68.
- [6] Neil Shenvi, Julia Kempe, and K. Birgitta Whaley, "Quantum random-walk search algorithm," Phys. Rev. A 67, 052307 (2003).
- [7] Giuseppe Di Molfetta and François Debbasch, "Discrete-time quantum walks: Continuous limit and symmetries," Journal of Mathematical Physics 53, 123302 (2012).
- [8] Giuseppe Di Molfetta, Marc Brachet, and Fabrice Debbasch, "Quantum walks in artificial electric and gravitational fields," Physica A: Statistical Mechanics and its Applications 397, 157–168 (2014).
- [9] Pablo Arrighi, Vincent Nesme, and Marcelo Forets, "The dirac equation as a quantum walk: higher dimensions, observational convergence," Journal of Physics A: Mathematical and Theoretical 47, 465302 (2014).
- [10] Sauro Succi, François Fillion-Gourdeau, and Silvia Palpacelli, "Quantum lattice boltzmann is a quantum walk," EPJ Quantum Technology 2 (2015), 10.1140/epjqt/s40507-015-0025-1.
- [11] Mohamed Hatifi, Giuseppe Di Molfetta, Fabrice Debbasch, and Marc Brachet, "Quantum walk hydrodynamics," Scientific Reports 9 (2019), 10.1038/s41598-019-40059-x.
- [12] R. Au-Yeung, V. M. Kendon, and S. J. Lind, "Quantum smoothed particle hydrodynamics algorithm inspired by quantum walks," Physics of Fluids 37 (2025), 10.1063/5.0268240.

- [13] Andrew M. Childs, "On the relationship between continuous- and discrete-time quantum walk," Communications in Mathematical Physics 294, 581–603 (2009).
- [14] Vivek Wadhia, Nicholas Chancellor, and Viv Kendon, "Cycle discrete-time quantum walks on a noisy quantum computer," The European Physical Journal D 78 (2024), 10.1140/epjd/s10053-023-00795-2.
- [15] C. Huerta Alderete, Shivani Singh, Nhung H. Nguyen, Daiwei Zhu, Radhakrishnan Balu, Christopher Monroe, C. M. Chandrashekar, and Norbert M. Linke, "Quantum walks and dirac cellular automata on a programmable trapped-ion quantum computer," Nature Communications 11 (2020), 10.1038/s41467-020-17519-4.
- [16] C. A. Ryan, M. Laforest, J. C. Boileau, and R. Laflamme, "Experimental implementation of a discrete-time quantum random walk on an nmr quantum-information processor," Physical Review A 72 (2005), 10.1103/physreva.72.062317.
- [17] K. McInroy, N. Pearson, and J. D. Pritchard, "Benchmarking the algorithmic performance of near-term neutral atom processors," (2024), arXiv:2402.02127 [quant-ph].
- [18] G Pelegrí, A J Daley, and J D Pritchard, "High-fidelity multiqubit rydberg gates via two-photon adiabatic rapid passage," Quantum Science and Technology 7, 045020 (2022).
- [19] Dolev Bluvstein, Harry Levine, Giulia Semeghini, Tout T. Wang, Sepehr Ebadi, Marcin Kalinowski, Alexander Keesling, Nishad Maskara, Hannes Pichler, Markus Greiner, Vladan Vuletić, and Mikhail D. Lukin, "A quantum processor based on coherent transport of entangled atom arrays," Nature 604, 451–456 (2022).
- [20] Luísa Toledo Tude and Marcos César de Oliveira, "Decoherence in the three-state quantum walk," Physica A: Statistical Mechanics and its Applications 605, 128012 (2022).
- [21] Garreth Kemp, Ilya Sinayskiy, and Francesco Petruccione, "Lazy open quantum walks," Phys. Rev. A 102, 012220 (2020).
- [22] Nicolas Jolly and Giuseppe Di Molfetta, "Twisted quantum walks, generalised Dirac equation and Fermion doubling," The European Physical Journal D 77 (2023), 10.1140/epjd/s10053-023-00659-9.
- [23] Manami Yamagishi, Naomichi Hatano, Ken-Ichiro Imura, and Hideaki Obuse, "Proposal of multidimensional quantum walks to explore dirac and schrödinger systems," Phys. Rev. A 107, 042206 (2023).
- [24] Michael A Nielsen and Isaac Chuang, Quantum computation and quantum information (American Association of Physics Teachers, 2002).
- [25] Ernst Hellinger, "Neue begründung der theorie quadratischer formen von unendlichvielen veränderlichen," Journal für die reine und angewandte Mathematik 136, 210–271 (1909).
- [26] https://qiskit.org/documentation/stubs/qiskit.quantum_info.hellinger_fidelity.html, Accessed 14 October 2025
- [27] Vivien M Kendon, "A random walk approach to quantum algorithms," Philosophical Transactions of the Royal Society A: Mathematical, Physical and Engineering Sciences **364**, 3407–3422 (2006).
- [28] B. L. Douglas and J. B. Wang, "Efficient quantum circuit implementation of quantum walks," Phys. Rev. A 79, 052335 (2009).
- [29] Harry Levine, Alexander Keesling, Giulia Semeghini, Ahmed Omran, Tout T. Wang, Sepehr Ebadi, Hannes Bernien, Markus Greiner, Vladan Vuletić, Hannes Pichler, and Mikhail D. Lukin, "Parallel implementation of high-fidelity multiqubit gates with neutral atoms," Physical Review Letters 123 (2019), 10.1103/physrevlett.123.170503.
- [30] Adriano Barenco, Charles H. Bennett, Richard Cleve, David P. DiVincenzo, Norman Margolus, Peter Shor, Tycho Sleator, John A. Smolin, and Harald Weinfurter, "Elementary gates for quantum computation," Physical Review A 52, 3457–3467 (1995).
- [31] B. Nikolov, E. Diamond-Hitchcock, J. Bass, N. L. R. Spong, and J. D. Pritchard, "Randomized benchmarking using nondestructive readout in a two-dimensional atom array," Phys. Rev. Lett. 131, 030602 (2023).
- [32] Simon J. Evered, Dolev Bluvstein, Marcin Kalinowski, Sepehr Ebadi, Tom Manovitz, Hengyun Zhou, Sophie H. Li, Alexandra A. Geim, Tout T. Wang, Nishad Maskara, Harry Levine, Giulia Semeghini, Markus Greiner, Vladan Vuletić, and Mikhail D. Lukin, "High-fidelity parallel entangling gates on a neutral-atom quantum computer," Nature 622, 268–272 (2023).
- [33] Hannah J. Manetsch, Gyohei Nomura, Elie Bataille, Kon H. Leung, Xudong Lv, and Manuel Endres, "A tweezer array with 6100 highly coherent atomic qubits," (2025), arXiv:2403.12021 [quant-ph].
- [34] Cica Gustiani, Tyson Jones, and Simon C. Benjamin, "The virtual quantum device (vqd): A tool for detailed emulation of quantum computers," Quantum 9, 1642 (2025).
- [35] Josias Old, Stephan Tasler, Michael J. Hartmann, and Markus Müller, "Fault-tolerant stabilizer measurements in surface codes with three-qubit gates," (2025), arXiv:2506.09029 [quant-ph].

A. $\,$ QW circuits with native gates of maximum rank 3

1. 1q-coin QWs

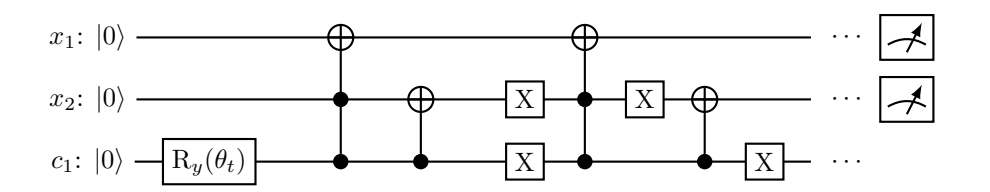


Figure 11: Gate circuit for quantum walk on a 4-node ring with single qubit coin.

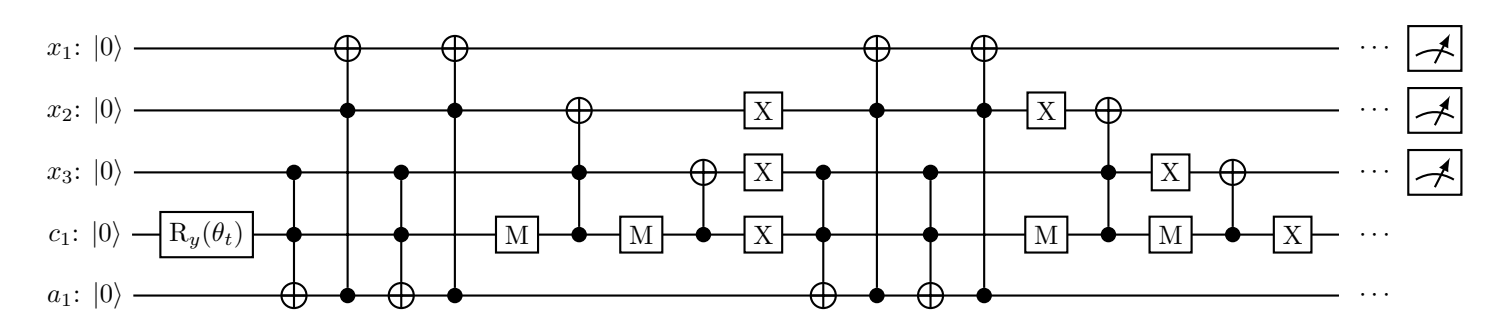


Figure 12: Max 3-qubit gate decomposition circuit for 1D non-lazy 8-node quantum walk.

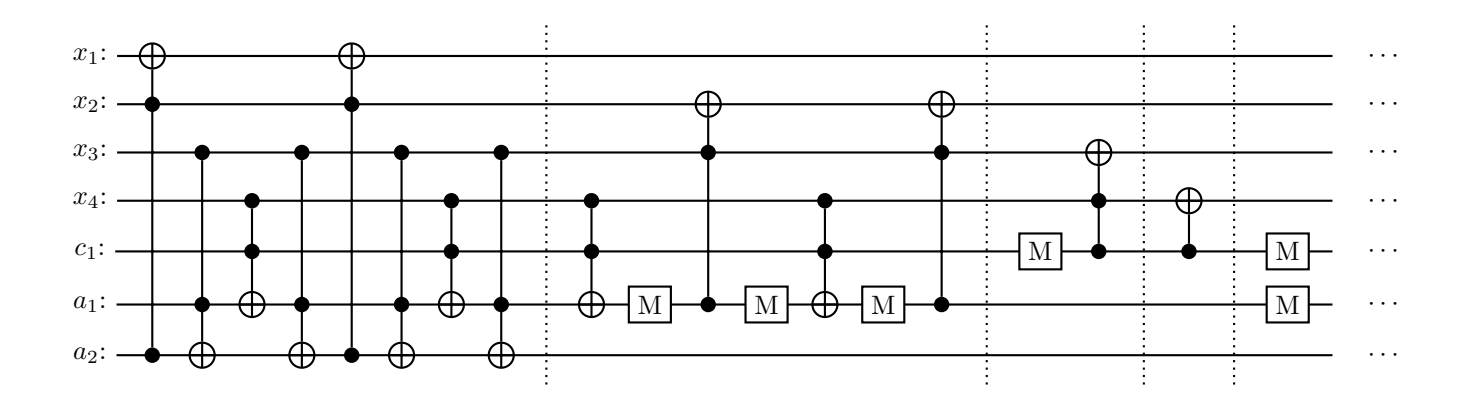


Figure 13: Gate circuit for 1D non-lazy 16-node quantum walk, INCREMENT ONLY.

2. 2q-coin QWs

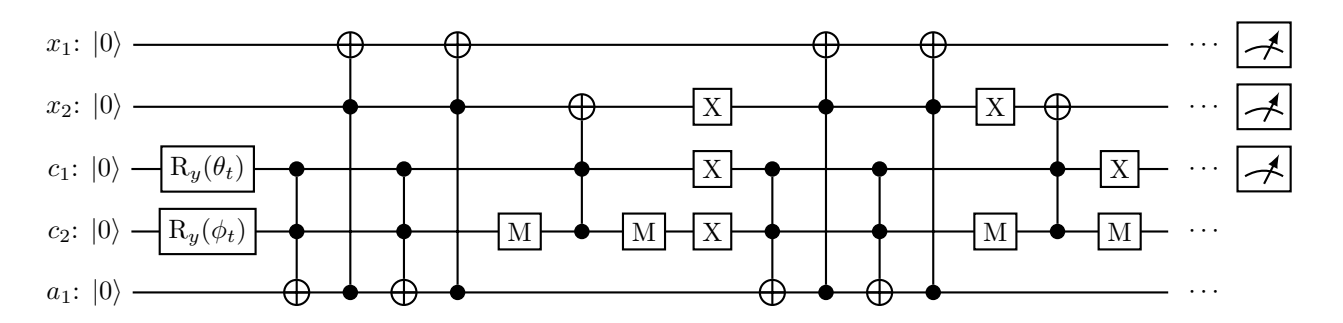


Figure 14: Max 3-qubit gate decomposition circuit for 1D lazy 4-node quantum walk.

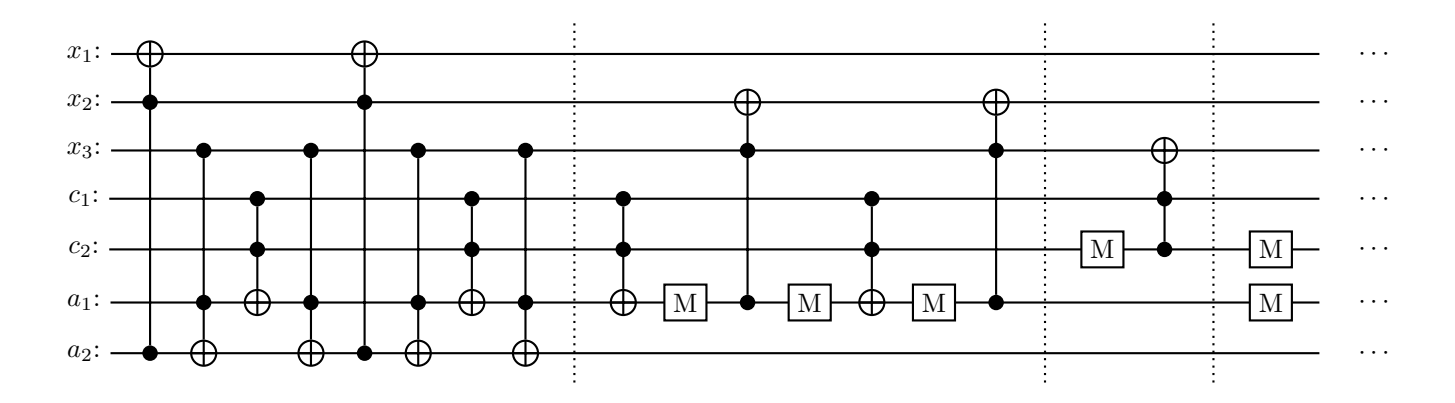


Figure 15: Max 3-qubit gate circuit for 1D lazy 8-node quantum walk, INCREMENT ONLY.

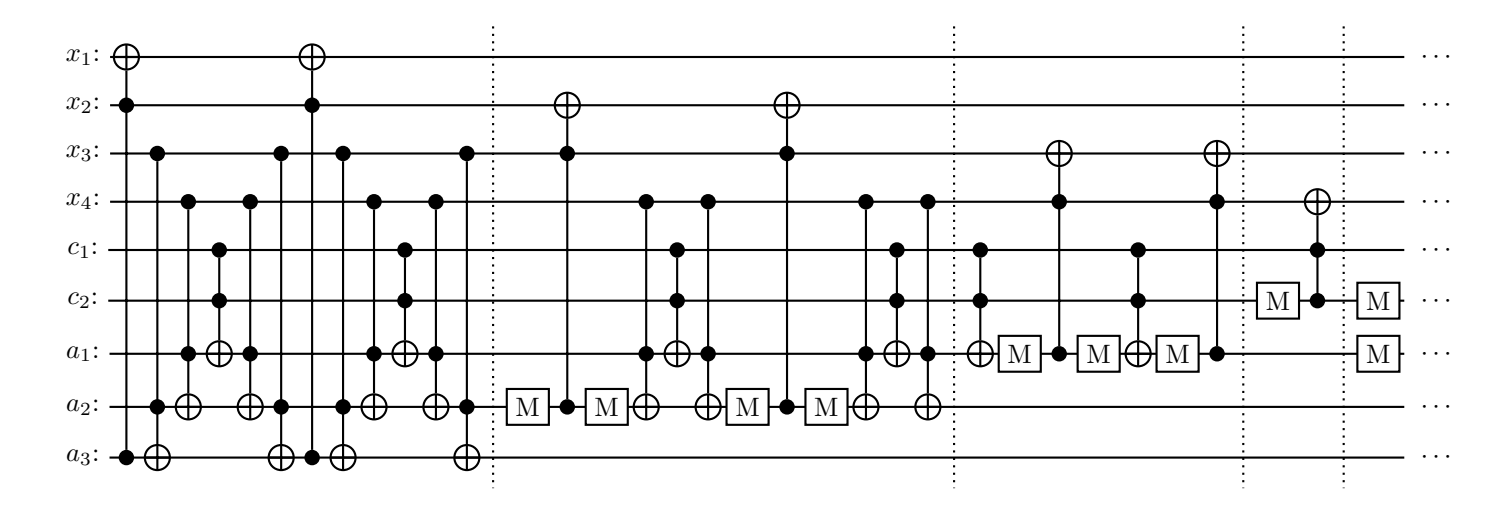


Figure 16: Max 3-qubit gate circuit for 1D lazy 16-node quantum walk: INCREMENT ONLY.

B. $\,$ QW circuits with native gates of maximum rank 4

1. 1q-coin QWs

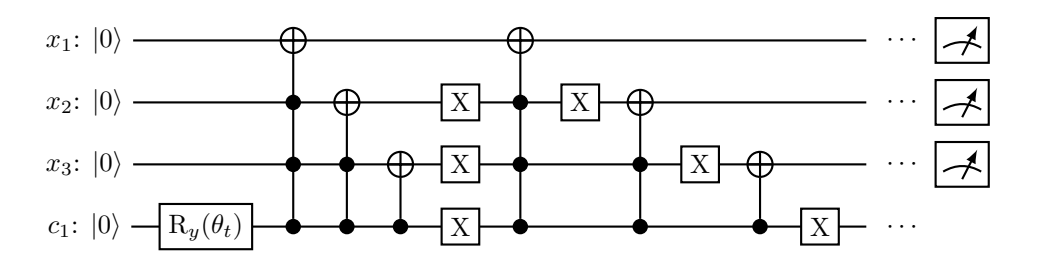


Figure 17: Max 4 gate circuit for 1D non-lazy 8-node quantum walk.

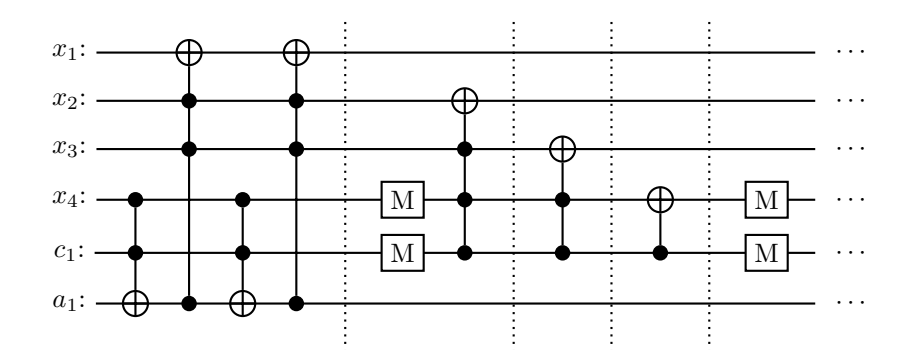


Figure 18: Gate circuit for 1D non-lazy 16-node quantum walk, INCREMENT ONLY.

2. 2q-coin QWs

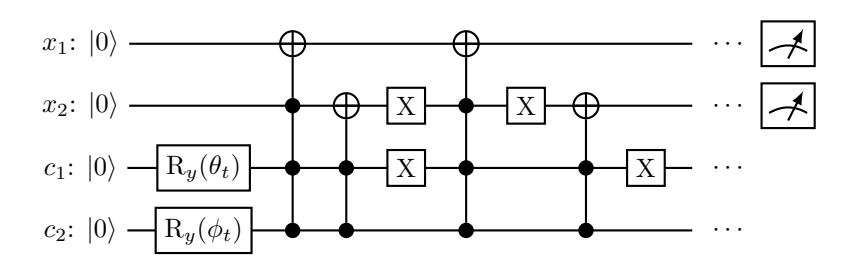


Figure 19: Max 4-qubit gate circuit for 1D lazy 4-node quantum walk.

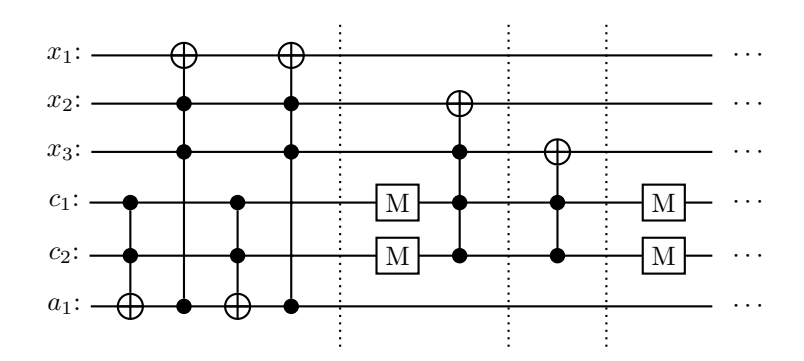


Figure 20: Max 4-qubit gate circuit for 1D lazy 8-node quantum walk, INCREMENT ONLY.

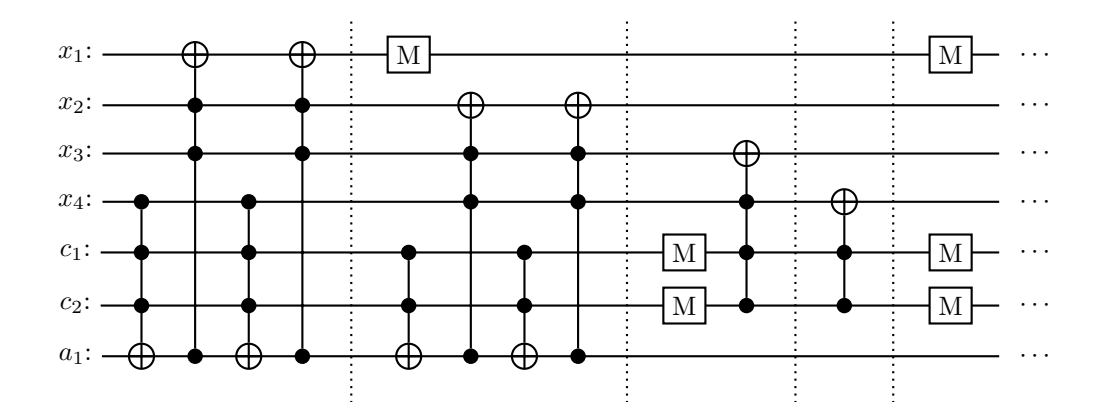


Figure 21: Max 4-qubit gate circuit for 1D lazy 16-node quantum walk, INCREMENT ONLY.